nature climate change
SUPPLEMENTARY INFORMATION
DOI: 10.1038/NCLIMATE2605

Decadal modulation of global surface temperature by internal climate variability

Aiguo Dai, John C. Fyfe, Shang-Ping Xie, and Xingang Dai

S1. Brief summary of the methodology

We first estimated the response of global-mean surface temperature (T) to historical forcings using the ensemble mean of the 66 all-forcing "historical" runs from 33 CMIP5 models[1] (http://cmip-pcmdi.llnl.gov/cmip5/index.html). Variations and changes associated with this estimate of the forced T time series were then removed from the observed T series at each grid point through linear regression (see Section S2). The residual T anomaly fields, referred to as detrended T, were then subjected to an Empirical Orthogonal Function (EOF) analysis (Section S5) in order to examine the contribution of the leading modes of the internal climate variability (ICV) to decadal global warming rates. Since the majority of the externally-forced signal was removed through the detrending, we consider the detrended T fields to consist of primarily unforced ICV. This detrending procedure (Section S3) using the CMIP5-simulated response is a key feature of our analysis. It reduces the chances for the externally-forced and unforced signals to mix up in the EOF expansion. An evaluation of this detrending method is presented in Section S3.

We emphasize that other detrending methods (e.g., linear detrending or using other time series[2-3]) are unlikely to remove most of the forced signal and produce a residual that can be considered as mostly ICV. Also, the spatial patterns of the leading EOFs may look similar with or without detrending (or using other detrending methods), but there are subtle differences in the EOF patterns and PC series that affect their contributions to the global-mean T series, as discussed below (Section S5).

Since our focus is on the decadal variations in global-mean T, not the overall warming rate over the entire analysis period from 1920 to 2013, we remove a warming bias in the average model-simulated global-mean T series through re-scaling. The impact of this removal on our results is examined in Section S4.

S2. Linear regression analysis

Let $T(n,i)$ be the surface temperature annual anomaly (ΔT) at grid point i for year n from observations, where n=1, ..., N=94 for 1920-2013. Let an over bar denote the area-weighted average over the globe from 60°S-75°N, and $\overline{T}(n)$ be the global-mean of $T(n,i)$ from observations, and $\overline{T_m}(n)$ be the global-mean surface air temperature annual anomaly for year n from the CMIP5 multi-model ensemble mean of historical simulations (for 1919-2005) plus RCP4.5 simulations (for 2006-2013). For simplicity, we assume that the mean for the whole analysis period (1920-2013) is removed in all the ΔT series so that the intercept is zero and can be ignored in all the linear regression equations listed below.

Generally, each ΔT series may be considered as consisting of an externally-forced component (denoted by subscript F, due to GHGs, aerosols, solar cycles and other external forcing) and an unforced component (denoted by subscript I, due to internal climate variability). For the global-mean ΔT from observations, we have

$$\overline{T}(n) = \overline{T_F}(n) + \overline{T_I}(n)\ . \tag{1}$$

Since the internal variations among individual realizations are usually uncorrelated and thus are averaged out over a large number of ensemble members, the global mean $\overline{T_m}(n)$ from the large CMIP5 ensemble contains mostly the externally-forced response to the historical external forcing changes with little internal variation. Despite various deficiencies in CMIP5 model physics and external-forcings, $\overline{T_m}(n)$ still provides a reasonable fit to the overall warming trend during 1920-2013 [$\overline{T}(n)$ from GISTEMP vs. $\overline{T_m}(n)$: r=0.96, slope $\overline{b_F}$=0.863] and arguably represents our best estimate of the temporal evolution of the response to historical external-forcings. Thus, we estimate $\overline{T_F}(n)$ using

$$\overline{T_F}(n) = \overline{b_F}\ \overline{T_m}(n)\ , \tag{2}$$

where $\overline{b_F}$ is the regression slope in $\overline{T}(n) = \overline{b_F}\,\overline{T_m}(n)$ + ε (residual). The unforced component can then be estimated as

$$\overline{T_I}(n) = \overline{T}(n) - \overline{b_F}\ \overline{T_m}(n)\ . \tag{3}$$

This definition ensures that $\overline{T_F}(n)$ and $\overline{T_I}(n)$ are uncorrelated, as any part in $\overline{T}(n)$ that is correlated with $\overline{T_m}(n)$ is removed through (3). We note that $\overline{T_I}(n)$ may still contain some small externally-forced changes that the CMIP5 ensemble mean may have missed and that are not correlated with $\overline{T_m}(n)$, although $\overline{b_F}\,\overline{T_m}(n)$ should account for the majority of the externally-forced changes in the historical ΔT record. Thus, we consider $\overline{T_I}(n)$ as primarily consisting of unforced, internally-generated variations.

The focus of this study is to examine the temporal evolution of $\overline{T_I}(n)$ and the spatial patterns associated with $\overline{T_I}(n)$, and any physical or statistical modes of variability that may contribute to this unforced component in the global-mean ΔT series. In particular, the role of these leading modes in explaining decadal variations of the global warming rate, including the warming hiatus during the most recent decade, is investigated.

Similar to $\overline{T}(n)$, the local ΔT series $T(n,i)$ may be considered as consisting of an externally-forced [$T_F(n,i)$] and an unforced internal [$T_I(n,i)$] component, and each of these components may be further separated into a part that is associated with their global counterpart and a local component, i.e.,

$$T_F(n,i) = b'_F(i)\,[\overline{b_F}\ \overline{T_m}(n)] + \varepsilon_F(n,i) = b_F(i)\ \overline{T_m}(n) + \varepsilon_F(n,i)\,, \tag{4}$$

$$T_I(n,i) = b_I(i)\ \overline{T_I}(n) + \varepsilon_I(n,i)\,, \tag{5}$$

$$T(n,i) = b_F(i)\ \overline{T_m}(n) + b_I(i)\ \overline{T_I}(n) + \varepsilon_F(n,i) + \varepsilon_I(n,i)\,, \tag{6}$$

where $\varepsilon_I(n,i)$ and $\varepsilon_F(n,i)$ contain, respectively, any local variability and local response to external forcing changes that are not accounted for by the global signals. The coefficients $b_F(i)$ and $b_I(i)$ are estimated using following regressions:

$$\mathrm{T}(n,i) = b_F(i)\ \overline{T_m}(n) + \varepsilon \qquad \text{and} \tag{7}$$

$$T'(n,i) \equiv T(n,i) - b_F(i)\ \overline{T_m}(n) = b_I(i)\ \overline{T_I}(n) + \varepsilon\,. \tag{8}$$

We refer to $T'(n,i)$ as the detrended ΔT field, which may include some externally-forced local response ($\varepsilon_F(n,i)$). However, by construction, the global means of the $\varepsilon_F(n,i)$ and $\varepsilon_I(n,i)$ are zero (i.e., they do not affect the global-mean ΔT), and the global mean of $b_F(i)$ is $\overline{b_F}$, while the global mean of $b_I(i)$ is one.

The spatial patterns of the regression coefficients $b_F(i)$ (Fig. S9a) reveal how the externally-forced global warming signal [$\overline{T_m}(n)$] projects onto the observed ΔT fields. Similarly, the patterns of $b_I(i)$ (Fig. S9d) depict how the unforced global internal variations [$\overline{T_I}(n)$] project onto the observed ΔT fields. Differences in these patterns provide insights into the different spatial structures associated with the externally forced and unforced components in the global-mean ΔT series. Figure S9 shows that the regression patterns associated with the externally forced and unforced global components are different (pattern correlation coefficient *r*=0.11), with the former resembling the pattern associated with the observed global-mean ΔT (Fig. S9b) and the latter (Fig. S9d) resembling the pattern associated with the IPO (Fig. 2c). The warming trend pattern from observations (Fig. S9b) includes both externally forced changes and unforced natural variations.

S3. Evaluation of the detrending procedure

To evaluate how well our detrending method performs in removing the externally-forced changes in individual simulations, we analyzed 40 historical simulations from one coupled model [namely, the Community Climate System Model version 4 (CCSM4)] with identical GHG and other external forcing changes[7]. We estimated the externally-forced component at each grid point using Eq. (4) for each model simulation, averaged over these 40 estimates, and then compared this realization-mean pattern with that computed directly as an average over the anomaly patterns from each of the 40 simulations (Fig. S10). Our method captures well the externally-forced signals (including volcanic) seen in the true ensemble mean. Similar results were also found for individual runs, although some spread is seen at high latitudes where the averaging area is small (Fig. S10c). Thus, our method of using CMIP5 ensemble mean and global mean [$\overline{T_m}(n)$] and local regression to estimate and remove the externally-forced signal in global ΔT fields appears to work well.

Our analysis (Fig. 4 and Fig. S3) of the 30-member ensemble of all-forcing historical runs by the CESM[4] (http://www.cesm.ucar.edu/experiments/cesm1.1/LE/) also suggests that our method seems to work well, as the ensemble-mean based detrending removes the forced signal in its run number 11, whose two leading EOFs account for the recent warming slowdown and other decadal variations in global-mean T. These model results are consistent with our analysis of the observed T, but in a cleaner setup with the forced response and unforced variations coming from the same model.

S4. Model mean biases and their impacts

We found that $\overline{b_F}$ =0.863 (0.762) in Eq. (2) for using the GISTEMP (HadCRUT4) observational data and the 66 simulations from 33 CMIP5 models. This suggests that this CMIP5 multi-model ensemble overestimates the overall warming from 1920-2013 by about 14% (24%) compared with that in the GISTEMP (HadCRUT4) dataset. This warming bias in the CMIP5 models has been noticed previously[8-9]. However, there are substantial differences in the long-term trends in the observational data sets, and $\overline{T_m}(n)$ varies among models with different climate sensitivities. These observational and model uncertainties make the assessment of the overall model warming bias difficult. While this systematic bias is of concern and affects the recent decadal warming rate in models, its impact on decadal T anomalies depend on the baseline period used to compute the T anomalies for both the observations and the models. For example, if one chooses the recent period from 2000 to 2013 as the baseline period, instead of the commonly used period from1961 to 1990, then the disagreement between the observed and simulated T anomalies since 2000 is much smaller than that shown in Fig. 1a. Since our focus is on decadal warming rates, we avoid these issues by removing this warming bias in models by rescaling the global-mean T from models using $\overline{b_F}$ (=0.863 for GISTEMP).

Figure S2 shows that without this rescaling, the most recent decade still shows a warming bias of about 0.1^{o}C even after accounting for the impact of ICV. As mentioned above, the magnitude of this bias in decadal T anomalies depends on the choice of the reference period and thus can be misleading. The more robust signal is the change rate of the T anomalies, which shows minimal warming since about 2000 for both observations and models with the two leading EOFs taken into account (black and blue lines in Fig. S2a). Thus, while the overall warming bias in the CMIP5 models induces a systematic difference between the observed and model-simulated global-mean T since about 2000, the warming hiatus (i.e., the change rate) during this period is largely accounted for by the two leading EOFs of ICV, with or without the rescaling.

We notice that the biases in model-simulated T response vary with individual forcings[10]. Here we used a single scaling factor to remove the overall bias in model global-mean T. It is straightforward to show that our scaling factor is a weighted average of the scaling factors for individual forcings under the following assumptions commonly used in optimal fingerprinting[11]: 1) the models can simulate the response to individual forcings, and 2) the response to individual forcings are additive. Let $y_i(n)$ be the response of the global-mean T for year n to forcing i in observations, and $x_i(n)$ be the model-simulated response to forcing i, and f_i is the scaling factor between the two so that $y_i(n)=f_i\, x_i(n)$. Since the responses are assumed to be additive, the total response is

$$y(n) = \sum_i y_i(n) = \sum_i f_i\, x_i(n) = f\, x(n)\,,$$

where $y(n)$ and $x(n)$ are the total response to all forcing in observations and models, respectively, and f is the overall scaling factor used in our analysis. It is clear that $f = \sum_i f_i\, x_i(n)/x(n) = \sum_i f_i\, x_i(n)/\sum_i x_i(n)$. Thus, our rescaling method is equivalent to estimating the response to individual forcings and then averaging them to derive the overall response to the total forcing. Our method does not necessarily imply that the scaling factors are the same for the responses to different forcings.

A similar argument applies to our detrending approach to remove the total response (i.e., $f\, x(n)$) from the observations, which is equivalent to estimating the response to each forcing (i.e., $f_i\, x_i(n)$) and then removing it from the observations. This is because the regressions employed here are linear and hence the response is additive.

S5. Empirical Orthogonal Function analysis

To further investigate the leading modes underlying the externally-unforced patterns shown in Fig. S9d and thus their impacts on the global-mean ΔT series, we performed an Empirical Orthogonal Function (EOF) analysis[12] of the detrended ΔT field $[T'(n,i)]$. Since $b_F(i)\,\overline{T_m}(n)$ accounts for the overwhelmingly large portion of the forced response at grid point i, removing this externally-forced component reduces the chance of contamination between the externally forced and unforced signals in the EOF decomposition. This is important given the relatively short record length of 94 years in our analysis compared against the time scales of the decadal to multi-decadal modes we are investigating.

As an alternative, we also performed an EOF analysis of the un-detrended ΔT field (i.e., $T(n,i)$) from observations, and found that the first EOF represents the global warming mode that essentially recovers the global-mean ΔT series $\overline{T}(n)$ (red line in Fig. S11a). As mentioned above, the unforced component [$\overline{T_I}(n)$] in the global-mean ΔT series is uncorrelated with the externally-forced component [$\overline{T_F}(n) = \overline{b_F}\ \overline{T_m}(n)$], thus the only possible reason for these two components to be mixed into one EOF mode has to be due to the similarity in their associated spatial patterns. To show this, we computed the following difference field:

$$\Delta T(n,i) = b(i)\,\overline{T}(n) - b_F(i)\;\overline{T_m}(n)\ , \tag{9}$$

where $b(i)$ is the slope in regression: $T(n,i) = b(i)\,\overline{T}(n) + \varepsilon$. Thus, $\Delta T(n,i)$ represents the difference between the ΔT associated with both the global externally forced and unforced components $[\overline{T_F}(n) + \overline{T_I}(n)]$ and that associated with the externally-forced component $[\overline{T_F}(n)]$ alone. In other words, $\Delta T(n,i)$ may be considered as the ΔT field associated with the internally-generated component in the global-mean ΔT series (but without local unforced variations, unlike $T'(n,i)$). To reveal the spatial patterns of $\Delta T(n,i)$, we first computed the global-mean $[\overline{\Delta T}(n)]$ of $\Delta T(n,i)$ and then its regression slope with local $\Delta T(n,i)$, i.e.,

$$\Delta T(n,i) = b_D(i)\,\overline{\Delta T}(n) + \varepsilon\ . \tag{10}$$

The spatial patterns of $b_D(i)$ (Fig. S9c) reveals that indeed they are similar to those associated with the global forced change (Fig. S9a; pattern correlation coefficient *r*=0.99). This leads to the merger of $\overline{T_F}(n) + \overline{T_I}(n)$ into the first principal component (PC1, Fig. S11a) whose spatial pattern (Fig. S11b) resembles the pattern associated with the global-mean ΔT (Fig. S9b), despite the fact that $\overline{T_F}(n)$ and $\overline{T_I}(n)$ are uncorrelated.

One might argue that the whole global-mean ΔT series (red line in Fig. S11a) should be considered as the externally-forced response since its projected spatial pattern (Fig. S9b) is similar to that associated with the externally-forced component (Fig. S9a). This would mean that there are no internal, unforced variations in the observed global-mean ΔT series. However, it is well known that the global-mean ΔT series from individual model runs contain unforced, random variations that lead to considerable differences among individual runs, and the ensemble mean is often the best estimate of the forced response[4,13]. Thus, the observed global-mean ΔT series is expected to contain some unforced variations, since the observations are sampled from one realization.

To show the differences in the EOFs for the undtrended and detrended ΔT fields, we write down the EOF expansions for both $T(n,i)$ and $T'(n,i)$, and denote the global warming or trend mode (Fig. S11a-b) as $\mathrm{eof_o}$ for the $T(n,i)$ case:

$$T(n,i) = pc_o(n)\,eof_o(i) + pc_1(n)\,eof_1(i) + pc_2(n)\,eof_2(i) + \cdots \tag{11}$$

$$T'(n,i) = PC_1(n)\,EOF_1(i) + PC_2(n)\,EOF_2(i) + \cdots \tag{12}$$

Since $T'(n,i) = T(n,i) - b_F(i)\;\overline{T_m}(n)$, we have

$$PC_1(n)\,EOF_1(i) + PC_2(n)\,EOF_2(i) + \cdots = [\,pc_o(n)\,eof_o(i) - b_F(i)\,\overline{T_m}(n)] + pc_1(n)\,eof_1(i) + pc_2(n)\,eof_2(i) + \cdots \tag{13}$$

We found that the PC_k and EOF_k (Fig. 2) of $T'(n, i)$ are similar to the pc_k and eof_k (Fig. S11) of $T(n, i)$, respectively, for the leading modes. However, there are some subtle differences between them that lead to non-zero global-mean values of the EOF_k coefficients, while the global-mean of the eof_k coefficients are close to zero. These differences result from the projection of the term $[\Delta T_{om}(n, i) \equiv pc_o(n)\, eof_o(i) - b_F(i)\, \overline{T_m}(n)]$ onto the spatial patterns of the leading modes (especially eof_1 and eof_4). When averaged globally, this term represents the observation-minus-model difference in their global-mean ΔT (black line in Fig. 1b), i.e.,

$$\overline{\Delta T}_{om}(n) = pc_o(n)\, \overline{eof_o\,(i)} - \overline{b_F}\, \overline{T_m}(n) \approx PC_1(n)\, \overline{EOF_1\,(i)} + PC_2(n)\, \overline{EOF_2(i)} + \cdots \quad (14)$$

Thus, the impact of all internally-generated climate variations ($\overline{\Delta T}_{om}(n)$) project onto the leading EOF_k of the detrended ΔT fields. This alters the original eof_k modes slightly such that they have non-zero global means. The higher-order EOFs from the detrended data show very small global means for their EOF coefficients (like in the un-detrended case), leading to small contributions to $\overline{\Delta T}_{om}(n)$.

In summary, we found that without the detrending of Eq. (8) (or detrending with the global-mean ΔT from observations), the leading EOF modes (besides the trend mode, Fig. S11) will not include the impacts of these modes on the global-mean ΔT, as their influences are either mixed up with the trend mode (due to the similarity of their spatial patterns), or contained in the global-mean ΔT series that is removed from the data. The detrending using Eq. (8) removes most of the externally forced changes in the observed ΔT fields, thus reducing the chance of mixing the externally forced changes and unforced variations in the EOF expansion. The impact of the internal variations on the global-mean ΔT should come primarily from the leading modes of variability and thus it is projected mainly onto the leading EOF modes.

References:

1. Taylor, K. E., R. J. Stouffer, and G. A. Meehl, 2012: An overview of CMIP5 and the experiment design. *Bull. Amer. Meteorol. Soc.*, **93,** 485-498.
2. DelSole, T., M.K. Tippett, J. Shukla 2011: A significant component of unforced multidecadal variability in twentieth century global warming. *J. Clim.*, **24**, 909-926.
3. Wu , Z., N.E. Huang, J.M. Wallace, B.V. Smoliak, X. Chen, 2011: On the time-varying trend in global-mean surface temperature. *Clim. Dyn.* **37**, 759–773.
4. Kay, J. E., C. Deser, A. Phillips, A. Mai, C. Hannay, G. Strand, J. Arblaster, S. Bates, G. Danabasoglu, J. Edwards, M. Holland, P. Kushner, J. -F. Lamarque, D. Lawrence, K. Lindsay, A. Middleton, E. Munoz, R. Neale, K. Oleson, L. Polvani, and M. Vertenstein, 2015: The Community Earth System Model (CESM) Large Ensemble Project: A Community Resource for Studying Climate Change in the Presence of Internal Climate

Variability. *Bull. Amer. Met. Soc.*, doi: http://dx.doi.org/10.1175/BAMS-D-13-00255.1, in press. [Article Download]

5. Hansen, J., R. Ruedy, M. Sato, and K. Lo, 2010: Global surface temperature change. *Rev. Geophys.* **48**, RG4004, doi:10.1029/2010RG000345.
6. Morice, C. P., J. J. Kennedy, N. A. Rayner, and P. D. Jones, 2012: Quantifying uncertainties in global and regional temperature change using an ensemble of observational estimates: The HadCRUT4 dataset, J. Geophys. Res., doi:10.1029/2011JD017187.
7. Mudryk, L.R., P.J. Kushner, and C. Derksen, 2013: Interpreting observed northern hemisphere snow trends with large ensembles of climate simulations. *Clim. Dyn.*, DOI 10.1007/s00382-013-1954-y.
8. Gillett, N. P., V. K. Arora, G. M. Flato, J. F. Scinocca, and K. von Salzen, 2012: Improved constraints on 21st-century warming derived using 160 years of temperature observations, *Geophys. Res. Lett*., 39, L01704, doi:10.1029/ 2011GL050226.
9. Fyfe, J. C., N. P. Gillett and F.W. Zwiers, 2013: Overestimated global warming over the past 20 years. *Nat. Clim. Change*, **3**, 767-769.
10. IPCC, 2013: Climate Change 2013: The Physical Science Basis. Contribution of Working Group I to the Fifth Assessment Report of the Intergovernmental Panel on Climate Change, edited by T. E. Stocker et al., Cambridge University Press, Cambridge, United Kingdom and New York, NY, USA.
11. Ribes, A., S. Planton and L. Terray: 2013: Application of regularized optimal fingerprinting to attribution. Part I: method, properties and idealized analysis. *Clim Dyn.* **41**: 2817–2836.
12. Monahan, A.H., J.C. Fyfe, M.H.P. Ambaum, D. Stephenson, and G.R. North, 2009: Empirical orthogonal functions: The medium is the message. *J. Climate*, **22** , 6501-6514.
13. Knutti, R., R. Furrer, C. Tebaldi, J. Cermak, and G. A. Meehl, 2010: Challenges in combining projections from multiple climate models. *J. Climate*, **23,** 2739-2758.

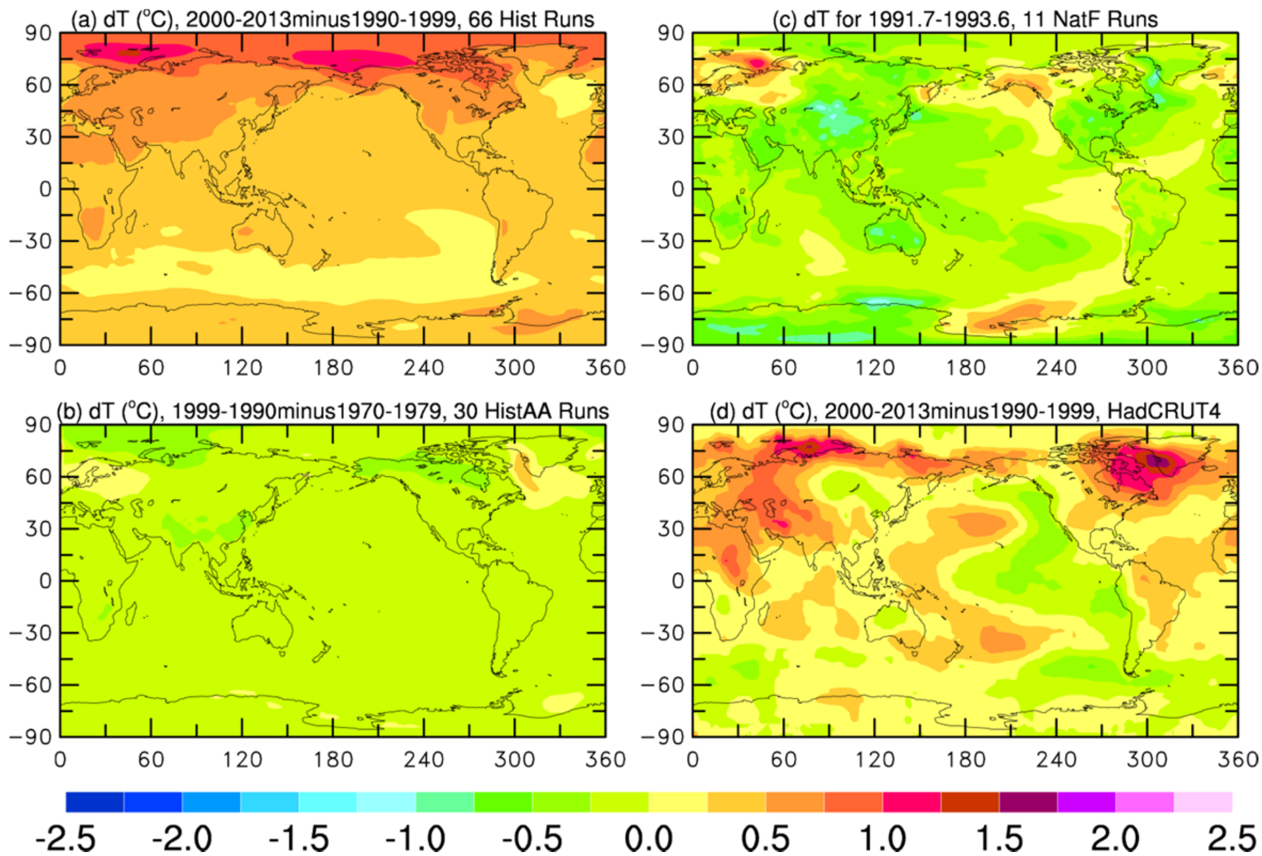

FIG. S1. Comparisons of the spatial patterns of the recent surface temperature changes. (**a**) 2000-2013 minus 1990-1999 difference of surface air temperature (Tas, in ^{o}C) from the ensemble mean of the 66 historical all forcing simulations by 33 CMIP5 models; (**b**) 1999-1990 minus 1970-1979 Tas difference from the ensemble mean of 30 historical anthropogenic aerosol forcing only simulations by 8 CMIP5 models; (**c**) Tas anomalies during July 1991-June 1993 (relative to the mean averaged over June 1988 - May 1991 and January 1994 - December 1996) after the Pinatubo volcanic eruption in June 1991 in the ensemble mean of 11 natural forcing only runs by 3 CMIP5 models (CCSM4, GFDL-CM3 and HaGEM2); and (**d**) the observed surface temperature difference between 2000-2013 and 1990-1999 based on the HadCRUT4 dataset[6]. This figure shows that the recent warming hiatus resulted from a cancellation of warming over most land areas and the Atlantic and Indian Oceans by cooling concentrated in the eastern Pacific Ocean, and that the temperature change patterns induced by recent volcanic or anthropogenic aerosol forcing or GHG increases are inconsistent with and thus cannot explain the observed temperature change patterns since the 1990s.

290

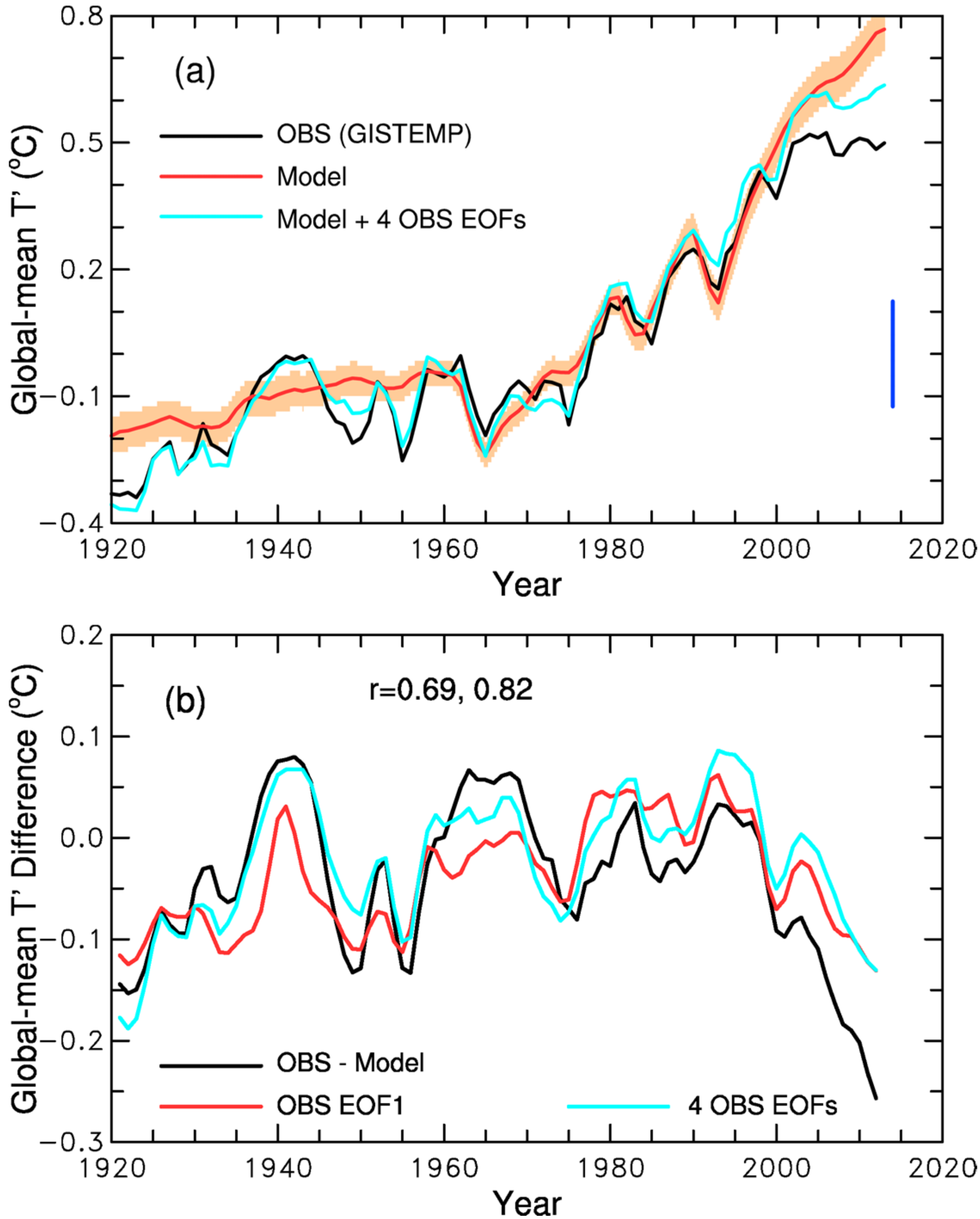

291

292 **FIG. S2**. Same as Fig.1 but without scaling the model-mean T (red line in **a**) by a factor of 0.863.

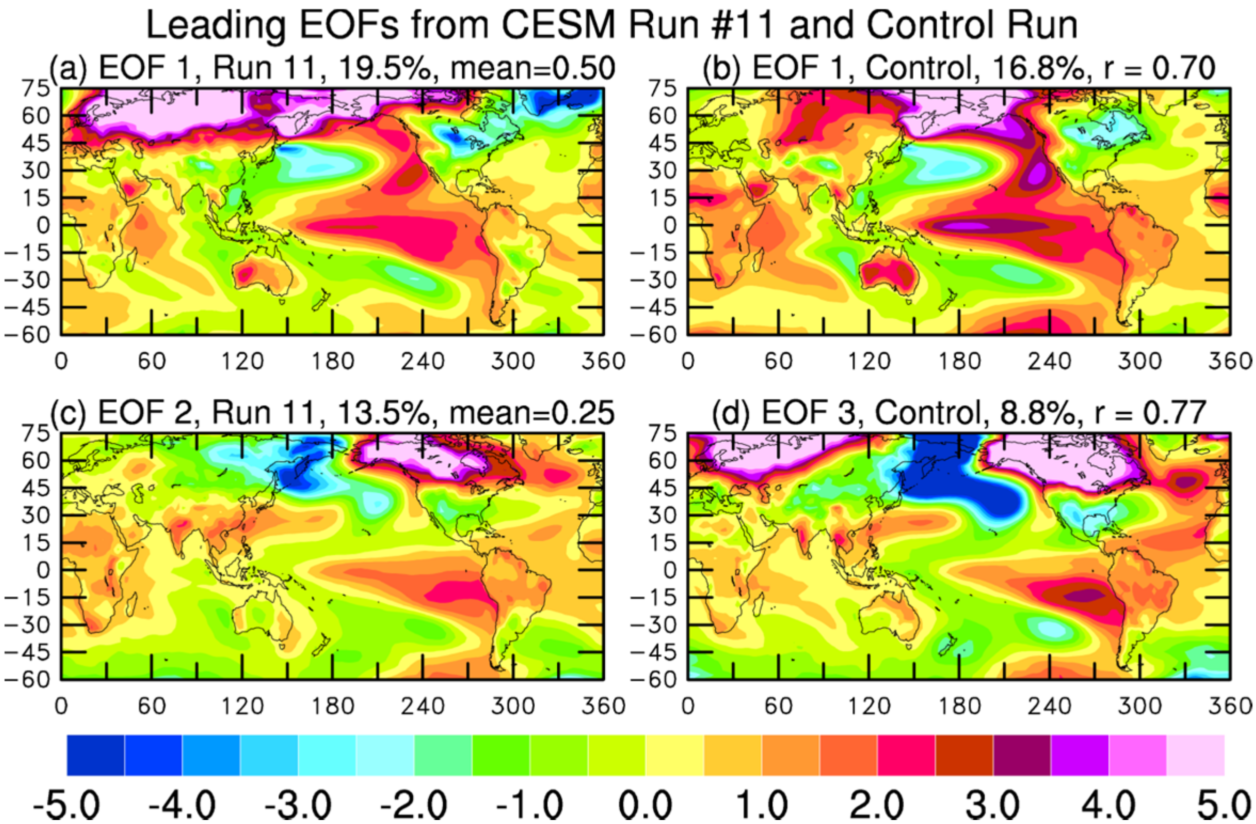

FIG. S3. **Comparison of the two leading EOFs** of the detrended T from CESM1 historical run number 11 (left column) and the similar EOFs of the T from a 550-year period of a control run (right column) by the same model[4]. The pattern correlation between the left and right panels of the same row is shown as *r* on top of panel (**b**) and (**d**). The % numbers are the % variance explained by the EOFs.

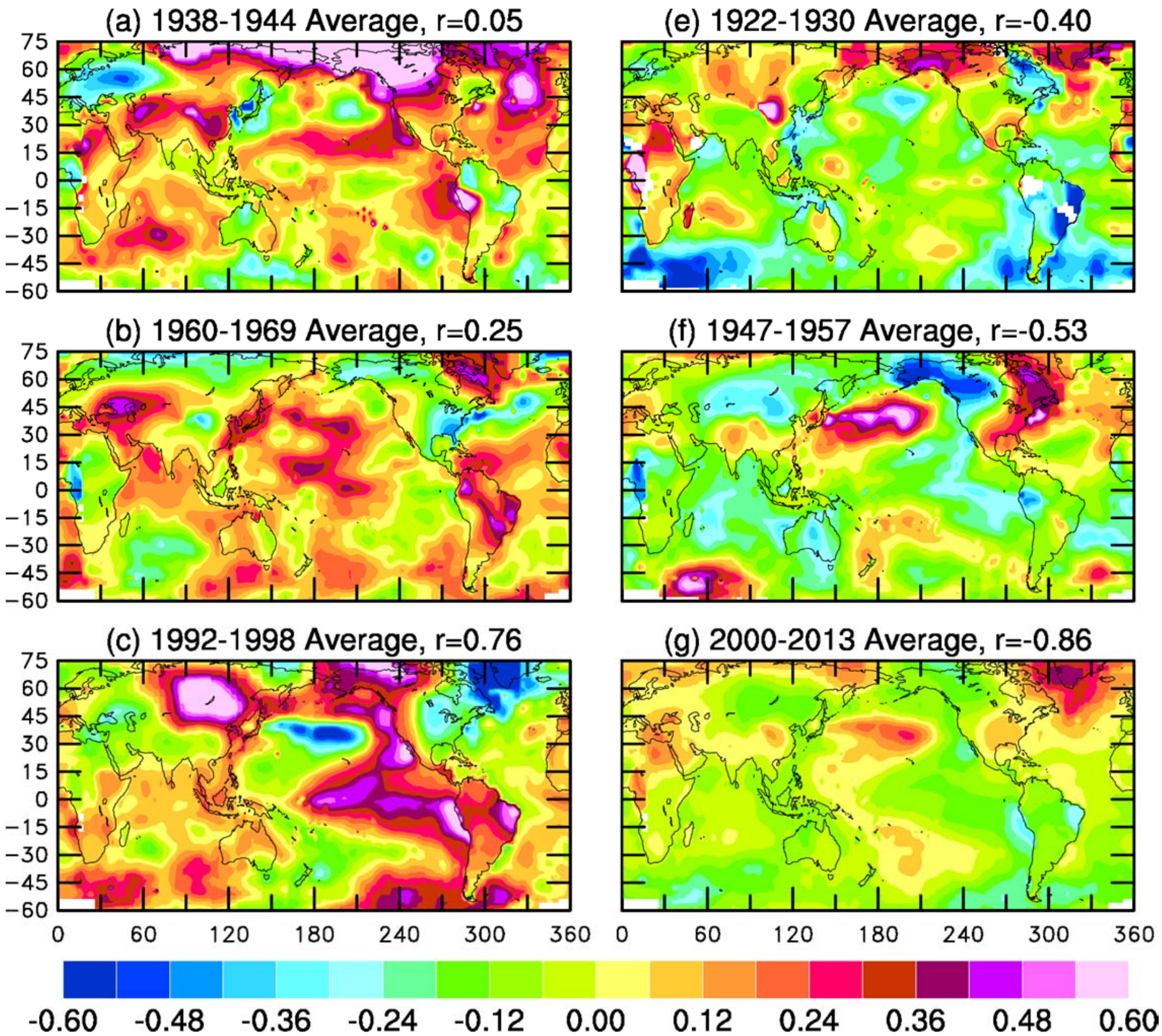

FIG. S4. **Spatial patterns of the warm (left) and cold (right) periods in the detrended GISSTEMP data set[5].** The CMIP5 multi-model ensemble global-mean surface air temperature anomalies were used to detrend the GISTEMP temperature anomalies at each box during 1920-2013 through linear regression (see SI). The anomalies (^{o}C) are relative to the 1961-1990 mean. The pattern correlation coefficient (*r*) with the IPO EOF (Fig. 2b) is shown on top of the panel.

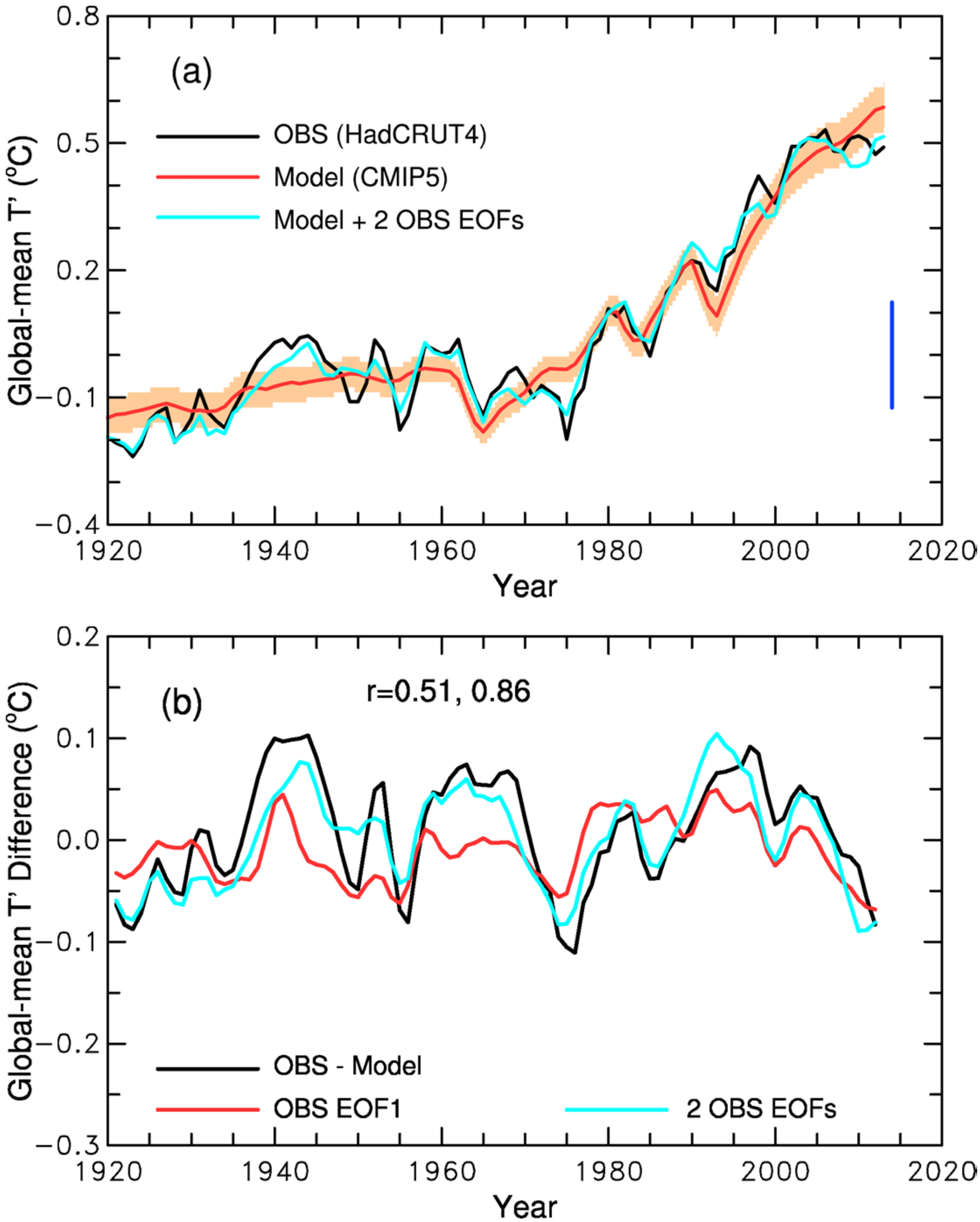

FIG. S5. Same as Fig. 1 but for using the HadCRUT4 data set[6] as the observations. The regression-derived scaling factor is 0.762, which is used to multiply the model-simulated anomaly series (red line).

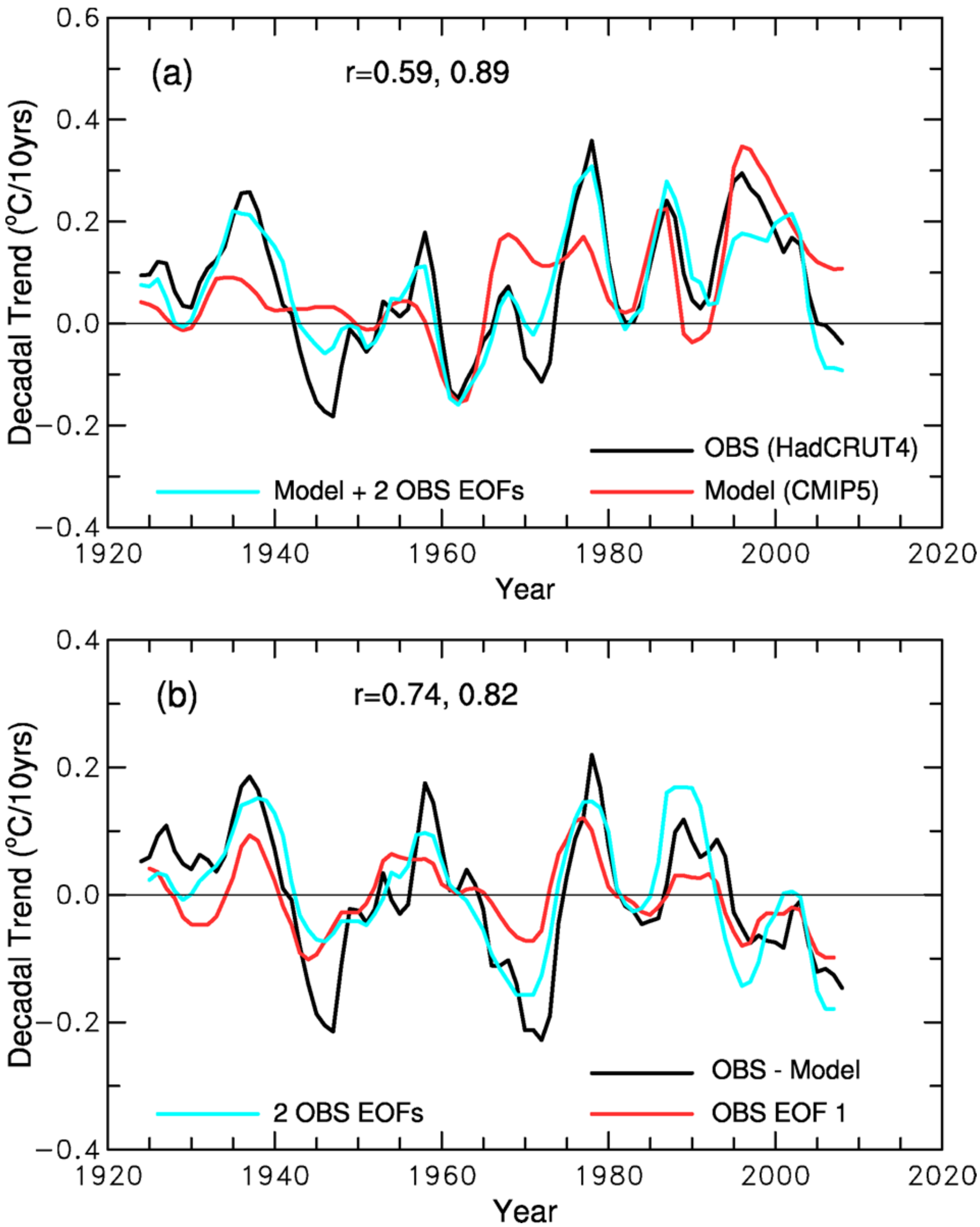

Fig. S6. Same as Fig. 3 but for using the HadCRUT4 as the observational data set.

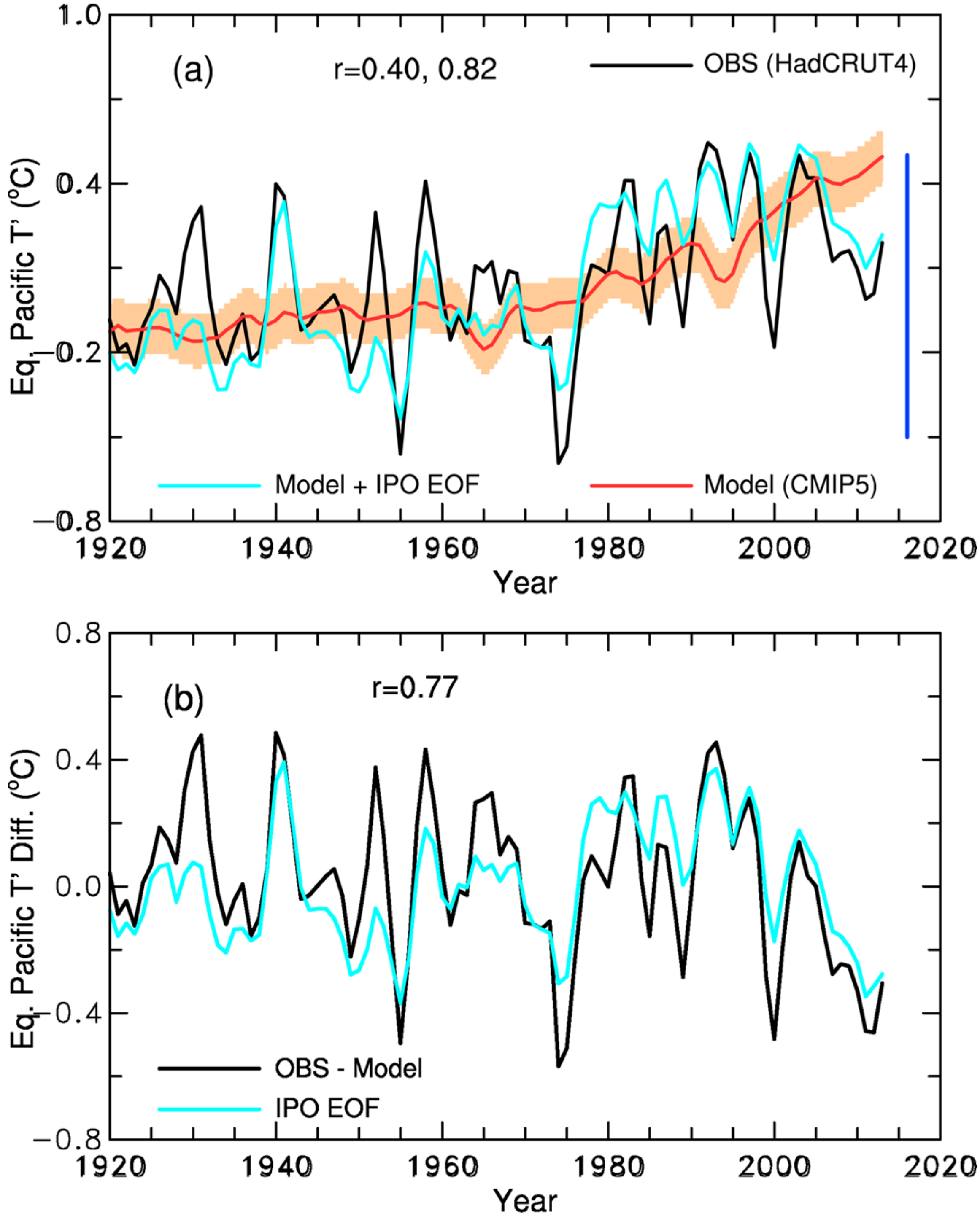

FIG. S7. Same as Fig. 5 but for using HadCRUT4 as the observational data set.

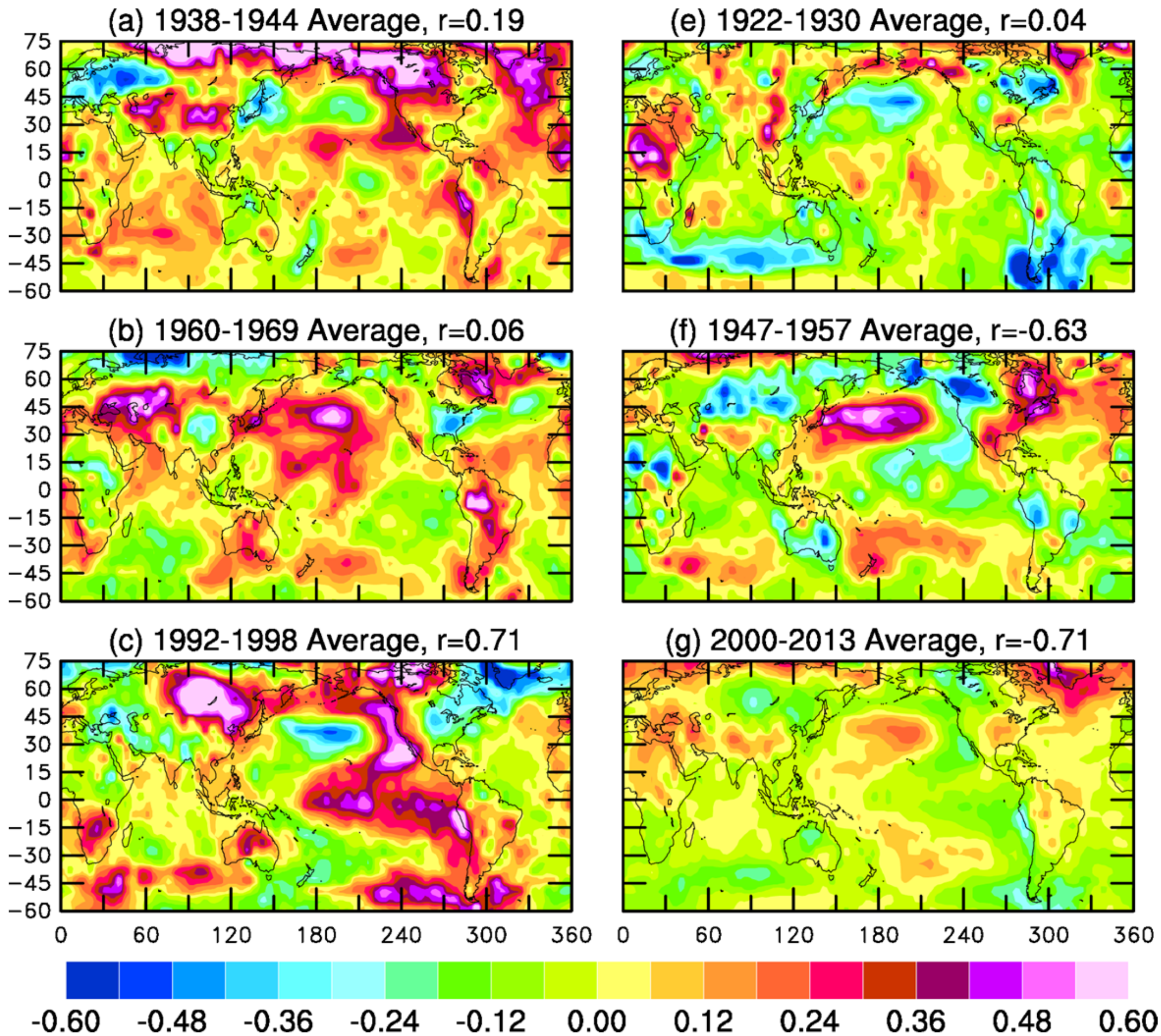

FIG. S8. Same as Fig. S4 but for using the HadCRUT4 data set.

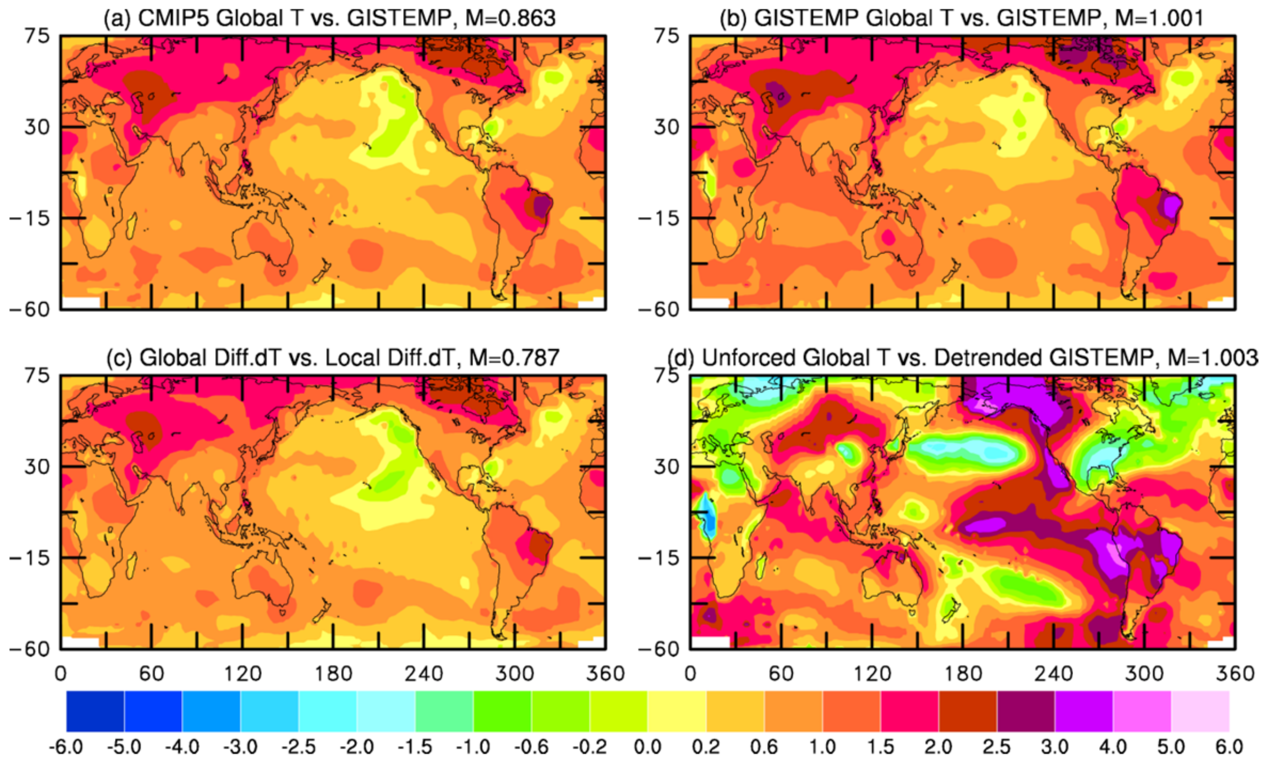

FIG. S9. Patterns of the regression coefficients. (**a**) between globally-averaged CMIP5 multi-model ensemble mean temperature anomalies (T') (as the x variable) and local T' series from GISTEMP data set ($b_F(i)$ in Eq. 6 in SI). (**b**) between the global-mean and local T' series from GISTEMP. (**c**) between the global-mean and local T' series of the difference field between the T' represented by panel (**b**) and (**a**) ($b_D(i)$ in Eq. 10 in SI). (**d**) between unforced global-mean T' and local detrended T' from GISTEMP ($b_N(i)$ in Eq. 6 in SI). The pattern correlation coefficient is 0.98 between (**a**) and (**b**), 0.99 between (**a**) and (**c**), and 0.11 between (**a**) and (**d**). The area-weighted global mean (M) is shown on top of each panel.

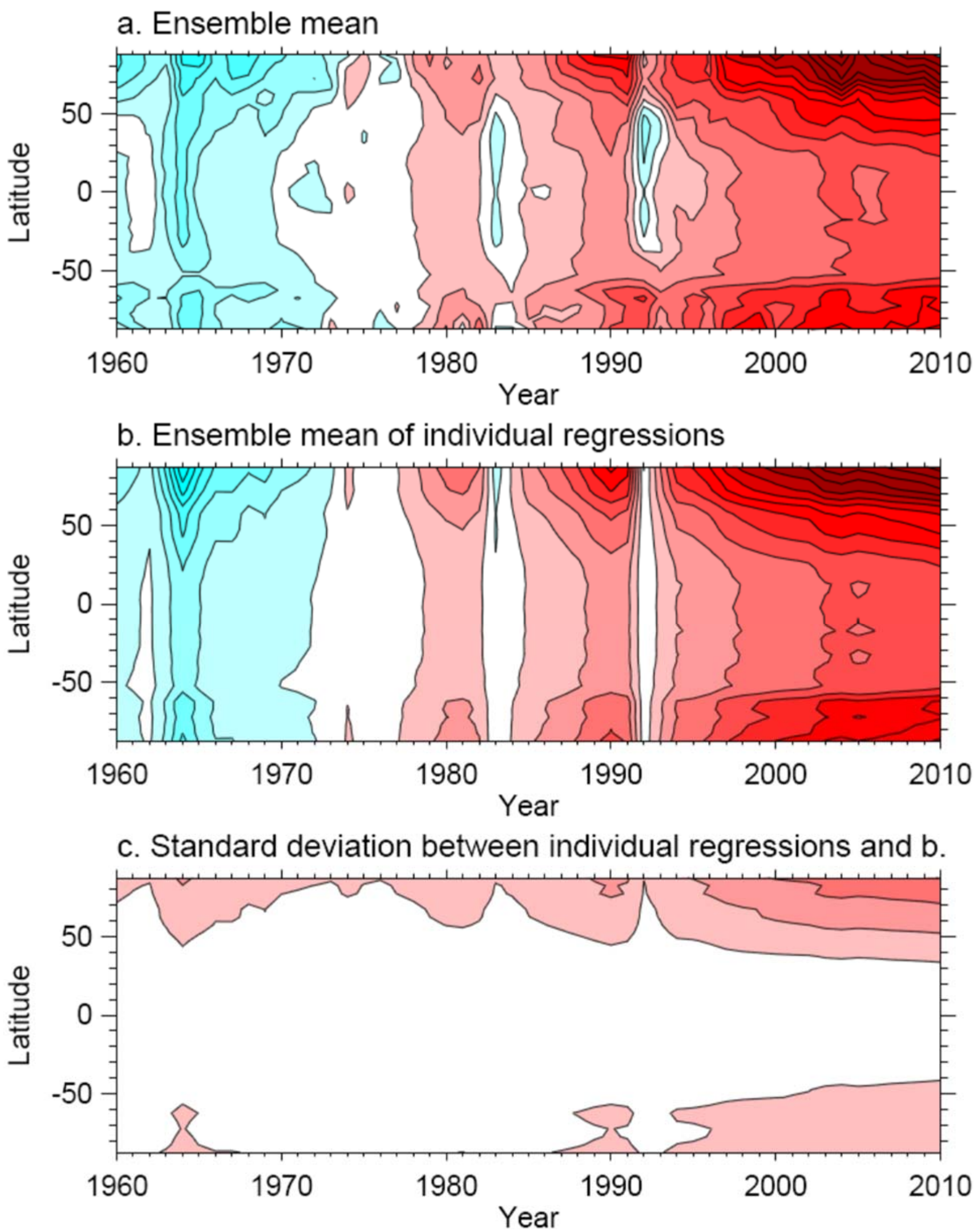

FIG. S10. Zonally-averaged surface air temperature anomalies (T', relative to the 1961-1990 mean) from1960-2010 from an ensemble of 40 historical simulations by a coupled model[2]. (**a**) 40 member ensemble mean of the model-simulated T'. (**b**) 40-member ensemble mean of the estimated T' using the global-mean T' series from the 40-member ensemble mean and its regression equation with local T' series for each member (cf. Eq. 4 in SI). (**c**) Standard deviation the regression-estimated T' among the individual runs. The contour interval is 0.15^{o}C and the contours are at ..., -0.375, -0.225, -0.075, 0.075, 0.225, 0.375^{o}C, ...

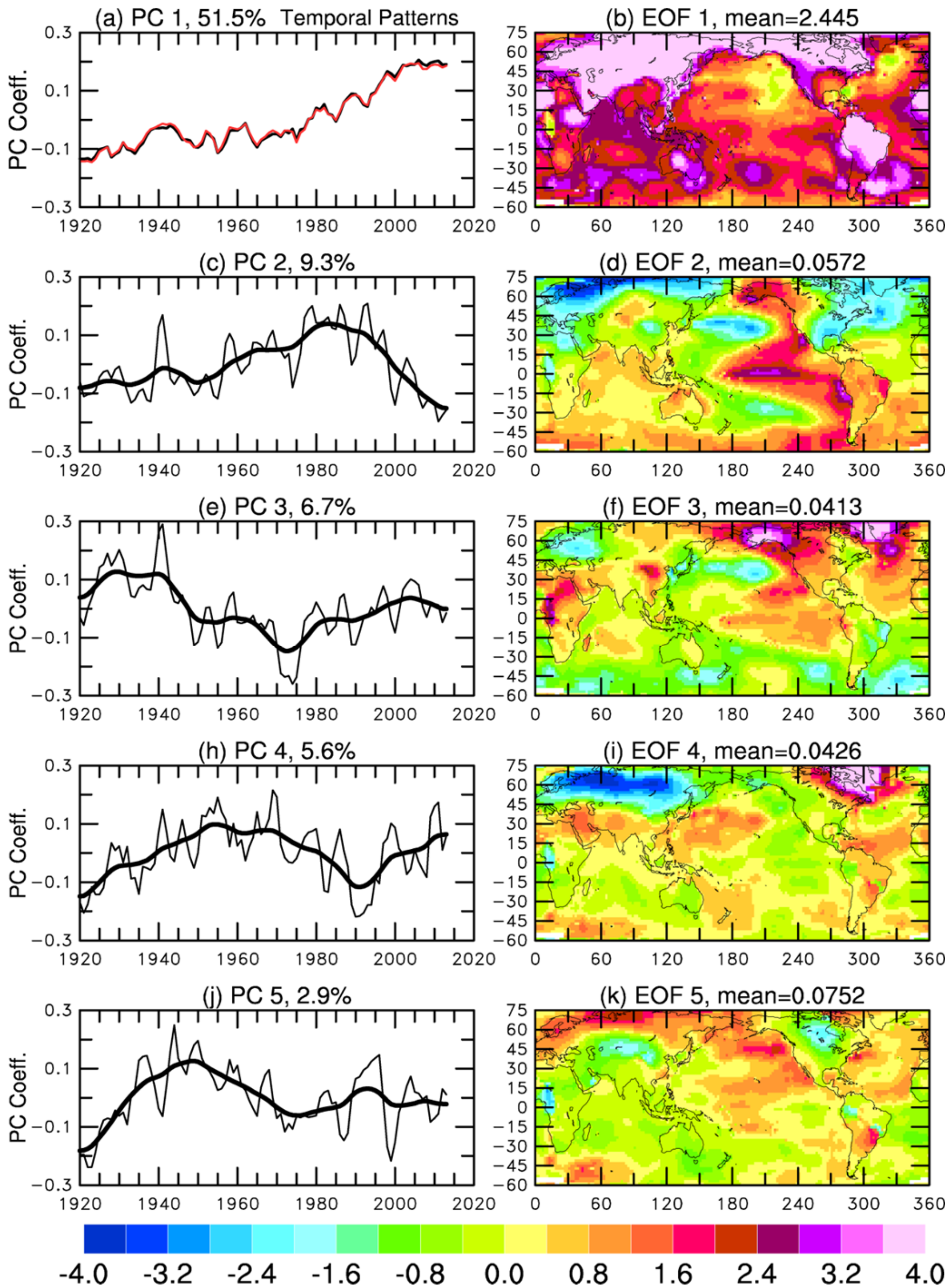

FIG. S11. The PCs (thick line is a smoothed curve as in Fig. 2a) and EOFs for the leading five EOF modes of the un-detrended GISTEMP data. Red line in (a) is the near-global (60°S-75°N) mean surface temperature anomalies in unit of 10 standard deviation (=2.53°C), i.e., for a reading of 0.1 on (a), the anomaly is 0.253°C.